Bayesian MR Tracking Algorithms

P. Gross[1], R. D. Darrow[1], C. L. Dumoulin[1]
[1]Imaging Technologies, GE GRC, Schenectady, NY, United States

Introduction

During MR tracking procedures signals are generated throughout the patient using a large transmit coil, but are detected with small receive coils. When a magnetic field gradient is applied the frequency of the signal depends directly on its position along that gradient. A typical receive coil only picks up MR signal from a small volume, thus resulting in data characterized by narrow frequency range which indicates the position of the coil.

However, determining the coil location is complicated by a number of factors. SNR is a function of coil and gradient orientation, availability of signal producing material, and losses in the coil and cable. Furthermore, at certain orientations the signal from a solenoid coil is dual-peaked and its width may vary from a single to several frequency intervals. Another commonly observed problem is coupling of tracking coils to surface, body and other tracking coils. Finally, susceptibility effects present in the frequency encoded data need to be removed when calculating the 3D coil position.

The motivation for this work is to further improve the reliability of MR tracking in anticipation of *in-vivo* intravascular human trials. New approaches to peak detection and data combination based on Bayesian statistic are explored. Data quality measures are introduced for use by the tracking system and to guide the user.

Methods

The probability that a set of modeling functions equals measured data plus Gaussian noise may be calculated using Bayesian statistics (Bretthorst 1988). In the algorithm developed here, the Fourier transformed data is modeled using *k*-space amplitudes from a range of frequencies characterized by a possible coil-position and a coil-width (see figure 1). In this fashion the probabilities for each candidate width and position may be determined. Averaging over the width dimension yields the probability as a function of frequency-position only. In order to avoid aliasing effects when calculating the expected position along the gradient (κ) and its uncertainty (standard-deviation σ) by integration, frequency is mapped onto a circle.

Based on the measured mean (κ) and standard deviation (σ), the 3D coil position may be calculated by assuming that the projection of the coil position onto the applied gradient has a Gaussian probability distribution. The probability distribution is then integrated over the susceptibility offset. The expected position vector (m) and covariance matrix (V) are then given by equations 1 and 2, where vectors g denote the gradients, subscripts i and j are the excitation numbers and N is the total number of excitations. With the standard deviations set to an arbitrary constant and the appropriate gradients, this method reduces to the "zero-gradient reference" and "Hadamard-encoded" cases (Dumoulin 1998).

The mean position and uncertainties may be calculated for a roadmap by vector transformations. The equation for an ellipsoid delineating the in-plane uncertainty boundary may then be obtained by integrating over the out-of-plane direction and plotted onto the roadmap (see image of contrast enhanced angiogram with intravenous injection, figure 2). The probability that a tracking coil is within the slice may also be assessed from the 3D distribution by integrating over the in-slice directions.

Simulated data were comprised of dual-peaked signal, interference, Gaussian noise and susceptibility offsets. The coil size of 2.0±0.5 mm, square FOV of 36 cm, a 256-by-256 image matrix and a 256 tracking matrix were assumed. Relative component strengths, peak widths and locations were sampled using Monte-Carlo methods.

Results and Conclusions

Up to a critical SNR and SIR (signal to interference ratio), the standard deviation of the errors were determined by the sampling rate and remained constant. Above SNR 4.5 or SIR 3.5, the root-mean-square (RMS) of the 3D predicted standard deviations equaled 1.7±0.2 pixels, while the RMS of the 3D error standard deviations was 1.6±0.1 pixels. The variation within and outside this range is shown in figure 3, where blue indicates the predicted values and red are the RMS simulated error standard deviations. The presented method therefore provided good estimates for high values of SNR and SIR, conservative estimates at lower SNR and SIR values, and unbiased means for all SNRs and SIRs.

Testing was performed mainly with simulated data, as it offered knowledge of the "true" coil positions and dynamic control over the signal, noise and interference parameters. The robustness to noise, interference, and aliasing, as well as the tests performed with real data indicate that the algorithms should perform well in real life conditions.

Overall, the Bayesian formalism was found to provide a flexible and natural framework, which may be readily adapted to test different peak detection and reconstruction methods. Since many of the steps were achieved using analytical expressions, an algorithmic complexity sufficiently low for real-time processing can be achieved. Furthermore, as the method is able to readily incorporate gradient strengths, directions and excitation numbers determined at run time, it opens new possibilities for automatic signal-quality guided acquisitions.

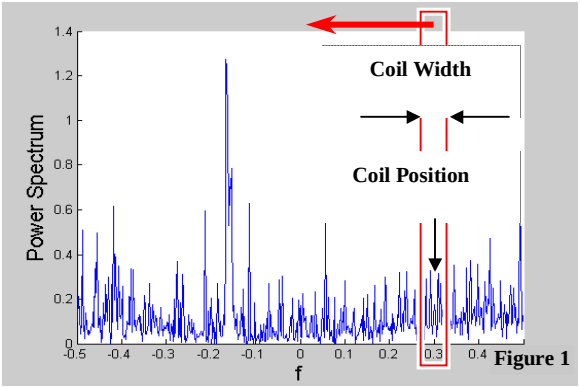

Figure 1

$$\mathbf{V}^{-1} = \sum_{i=1}^{N} \frac{\mathbf{g}_i^t}{\sigma_i^2} \left(\mathbf{g}_i - \sum_{j=1}^{N} \frac{\mathbf{g}_j}{\sigma_j^2} \Big/ \sum_{j=1}^{N} \frac{1}{\sigma_j^2} \right) \quad (1)$$

$$\mathbf{m} = \sum_{i=1}^{N} \frac{\kappa_i}{\sigma_i^2} \left(\mathbf{g}_i - \sum_{j=1}^{N} \frac{\mathbf{g}_j}{\sigma_j^2} \Big/ \sum_{j=1}^{N} \frac{1}{\sigma_j^2} \right) \mathbf{V} \quad (2)$$

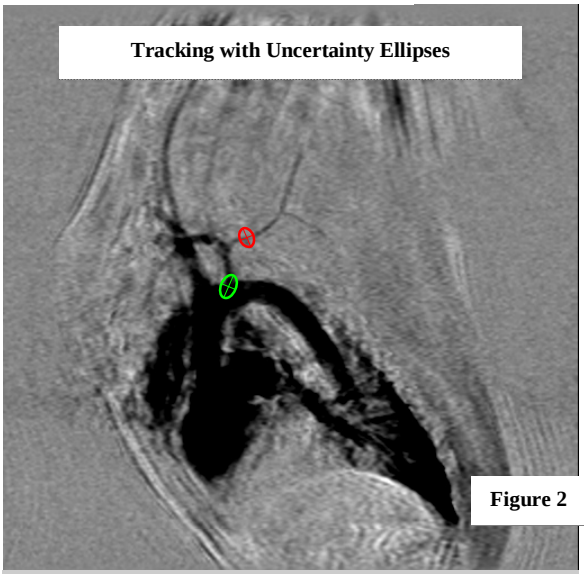

Figure 2

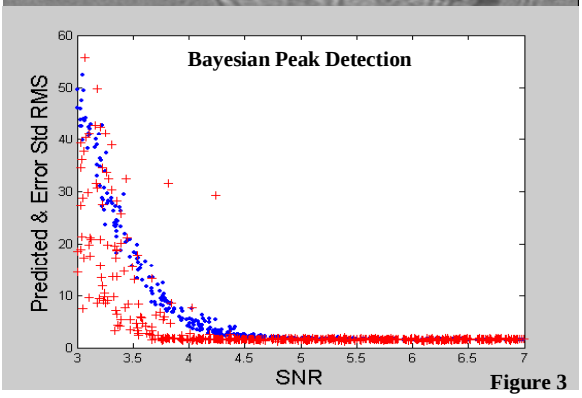

Figure 3

Bretthorst, G.L. *Bayesian Spectrum Analysis and Parameter Estimation*. Springer-Verlag, Berlin, Germany, 1988

Dumoulin, C.L. *Interventional MRI*. Chapter: Active Visualization. Springer-Verlag, Berlin, Germany, 1998.